

1 **U-Pb dating of middle Eocene-Pliocene multiple tectonic pulses in the Alpine**
2 **foreland**

3

4 **Luca Smeraglia^{1,2,3}, Nathan Looser^{4*}, Olivier Fabbri², Flavien Choulet², Marcel Guillong⁴,**
5 **Stefano M. Bernasconi⁴**

6

7 1. National Research Council, IGAG, Rome, Italy

8 2. Chrono-Environnement, UMR 6249, Université de Bourgogne-Franche Comté, 25000 Besançon, France

9 3. formerly at Dipartimento di Scienze della Terra, Sapienza Università di Roma, P.le Aldo Moro 5, 00185, Roma

10 4. Geological Institute, ETH Zürich, Sonneggstrasse 5, 8092 Zürich, Switzerland

11

12 *Corresponding author e-mail address: Nathan.looser@erdw.ethz.ch

13

14 **Abstract.** Foreland fold-and-thrust belts record long-lived tectono-sedimentary activity, from
15 passive margin sedimentation, flexuring, and further involvement into wedge accretion ahead of an
16 advancing orogen. Therefore, dating fault activity is fundamental for plate movement
17 reconstruction, resource exploration or earthquake hazard assessment. Here, we report U-Pb ages of
18 syntectonic calcite mineralizations from four thrusts and three tear faults sampled at the regional
19 scale, across the Jura fold-and-thrust belt in the northwestern Alpine foreland (eastern France).
20 Three regional tectonic phases are recognized in the middle Eocene-Pliocene interval: (1) pre-
21 orogenic faulting at 48.4 ± 1.5 and 44.7 ± 2.6 Ma associated to the far-field effect of the Alpine or
22 Pyrenean compression, (2) syn-orogenic thrusting at 11.4 ± 1.1 , 10.6 ± 0.5 , 9.7 ± 1.4 , 9.6 ± 0.3 , and
23 7.5 ± 1.1 Ma associated to the formation of the Jura fold-and-thrust belt with possible in-sequence
24 thrust propagation, and (3) syn-orogenic tear faulting at 10.5 ± 0.4 , 9.1 ± 6.5 , 5.7 ± 4.7 , and at $4.8 \pm$
25 1.7 Ma including the reactivation of a pre-orogenic fault at 3.9 ± 2.9 Ma. Previously unknown
26 faulting events at 48.4 ± 1.5 and 44.7 ± 2.6 Ma predate by ~ 10 Ma the reported late Eocene age for

27 tectonic activity onset in the Alpine foreland. In addition, we date the previously inferred re-
28 activation of pre-orogenic strike-slip faults as tear faults during Jura imbrication. The U-Pb ages
29 document a minimal time frame for the evolution of the Jura FTB wedge by possible in-sequence
30 thrust imbrication above the low-friction basal décollement consisting of evaporites.

31

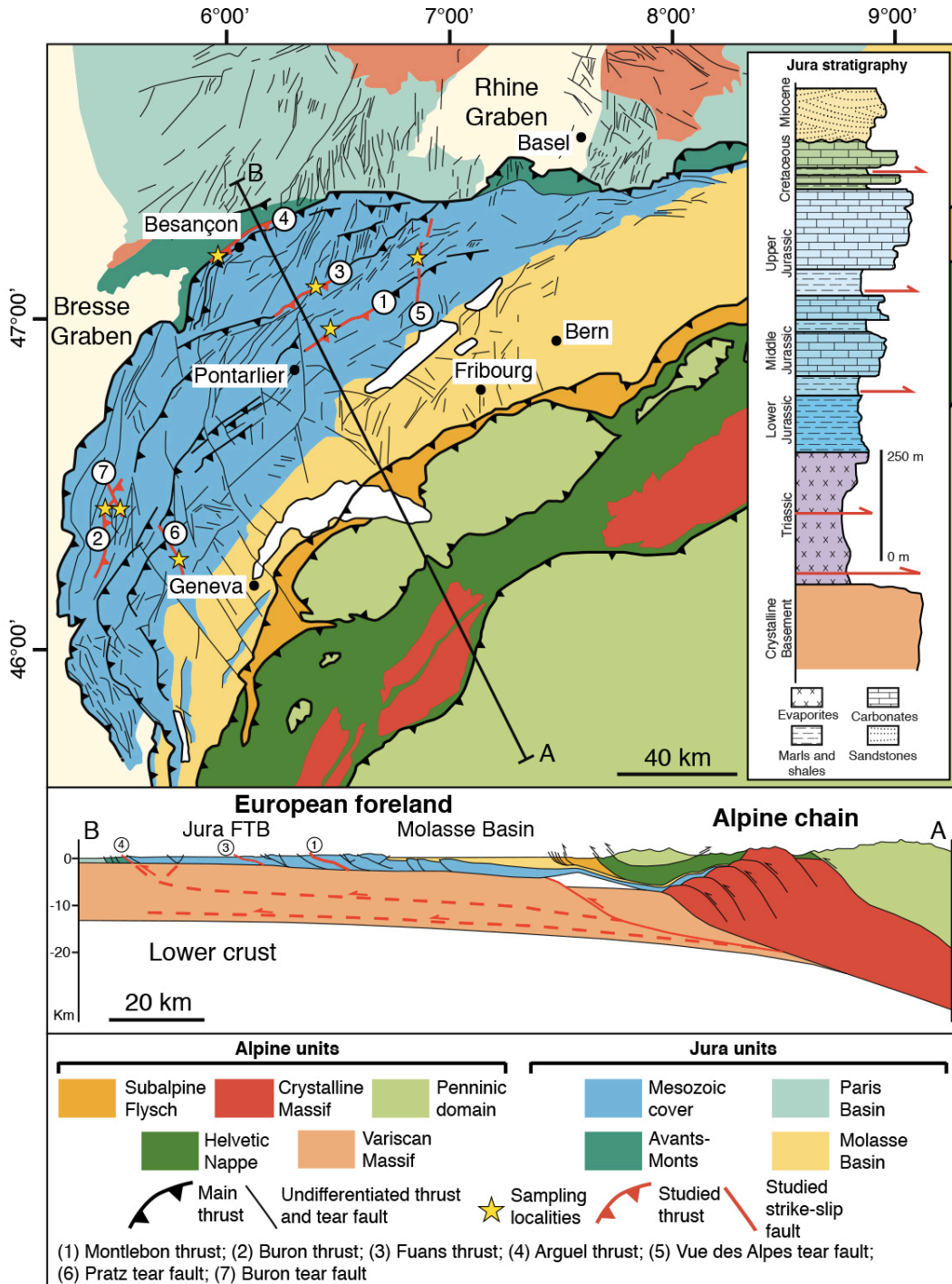
32 **1. Introduction**

33 Foreland fold-and-thrust belts develop at the external edges of orogens and are characterized
34 by a multiphase tectono-sedimentary history including: pre-orogenic sedimentation, uplift at the
35 peripheral bulge of the advancing orogen, progressively accelerating subsidence followed by syn-
36 tectonic sedimentation, and accretion of the sedimentary cover into the foreland fold-and-thrust belt
37 ([Lacombe et al., 2007](#)). Unraveling the timing of these tectonic events is fundamental for plate
38 kinematic modelling, natural resource exploration, paleoseismicity, and topography evolution
39 studies ([Vergés et al., 1992](#); [Craig and Warvakai, 2009](#)). However, deciphering the different
40 tectonic phases is complicated by the overprinting of inherited structures by progressively younger
41 tectonic events.

42 This issue is addressed by dating syn-tectonic sediments and, more recently, better
43 constrained through dating of fault activity with K-Ar, $^{40}\text{Ar}/^{39}\text{Ar}$, and U-Pb and U-Th methods ([Van
44 der Pluijm et al., 2009](#); [Vrolijk et al., 2018](#)). In particular, calcite U-Pb and U-Th geochronology
45 ([Roberts et al., 2020](#)) is the unique method for dating syntectonic calcite mineralizations. This
46 technique has been applied for dating single faults in extensional, strike-slip, and compressional
47 settings ([Goodfellow et al., 2017](#); [Nuriel et al., 2017](#); [Hansman et al., 2018](#); [Smeraglia et al., 2019](#);
48 [Carminati et al., 2020](#)). So far, the dating of multiple faults at the regional scale across a foreland
49 fold-and-thrust belt remains rare ([Beaudoin et al., 2018](#); [Looser et al., 2021](#)).

50 In this study, we dated syntectonic calcite mineralizations from four thrusts and three tear
51 faults sampled across the Jura fold-and-thrust belt (Jura FTB, eastern France, [Fig. 1](#)) by laser
52 ablation inductively coupled plasma mass spectrometry (LA-ICP-MS) U-Pb dating. We

53 reconstructed three tectonic phases having occurred in the middle Eocene-Pliocene period,
 54 documenting a long-lived polyphase tectonic history of the northwestern Alpine foreland system
 55 along the convergent boundary between European and African plates.



56
 57 **Figure 1.** Geological map of the northwestern Alpine foreland and surrounding areas and stratigraphic column of the
 58 main lithological units of the Jura area. Map modified from Rime et al. (2019), cross-section modified from Von Hagke
 59 et al., 2014.

60 2. Tectonic setting

61 Located in the Western Alps foreland, the Jura FTB formed by the ongoing continental
62 collision of the Eurasian plate with the African plate (Sommaruga, 1997; Mosar, 1999; Lacombe
63 and Mouthereau, 2002; Affolter and Gratier 2004; Bellahsen et al., 2014) (Fig. 1). Shortening
64 affected the Triassic-late Miocene sedimentary succession deposited on the European passive
65 margin above the Hercynian crystalline basement and caused brittle-ductile deformation at several
66 levels (Fig. 1) (Philippe et al., 1996; Homberg et al., 2002; Ustaszewski and Schmid, 2006). The
67 sedimentary succession starts with Triassic shales and evaporites overlain by Jurassic-Cretaceous
68 shales, marls, and limestones (Fig. 1) (Sommaruga et al., 2017). Following a Late Cretaceous-
69 Eocene regional unconformity, Oligocene-Miocene shallow marine to continental clastic deposits of
70 the Molasse Basin were deposited above Cretaceous limestones (Fig. 1).

71 The post-Mesozoic tectonic history of the Jura area is assumed to have started in the middle
72 Eocene with N-S shortening related to the far field effect of the "Pyrenean orogeny" generating
73 strike-slip faults (Bergerat, 1987). However, no absolute ages of this tectonic phase are available.
74 Based on structural analyses and calcite U-Pb ages, three phases of normal faulting during the Late
75 Eocene, Oligocene, and Miocene in the distal parts of the Molasse Basin in northern Switzerland
76 and in the Jura area have been documented (Lacombe et al., 1993; Homberg et al., 2002; Mazurek
77 et al., 2018; Radaideh and Mosar, 2021). Normal faulting during the Late Eocene-Oligocene is
78 associated to crustal extension due to the opening of the Rhine Graben (Lacombe et al., 1993;
79 Homberg et al., 2002; Mazurek et al., 2018; Radaideh and Mosar, 2021) or to the coeval onset of
80 Alpine collision (Merle and Michon, 2001), while normal faulting during the middle Miocene has
81 been related to crustal tilting associated to uplift of the Black Forest Highlands and subsidence of
82 the northern part of the Molasse Basin (Mazurek et al., 2018).

83 Biostratigraphic dating of syn-orogenic deposits, geomorphological observations,
84 interpretation of seismic reflection profiles, and syntectonic calcite U-Pb ages of fault activity in the
85 eastern tip of Jura FTB indicate that orogenic shortening started ~14.5 Ma ago (Langhian times) at

86 the latest (Looser et al., 2021 and references therein) and is still active (Mosar, 1999; Becker, 2000;
87 Lacombe and Mouthereau, 2002; Madritsch et al., 2008). Shortening was accommodated by N to NE-
88 verging and NE-SW-striking thrusts and by NW-SE to N-S trending sinistral tear faults
89 (Sommaruga, 1997) (Fig. 1). The main décollement level of the thrust system developed along
90 Triassic evaporites (Jordan, 1992; Pfiffner, 2014; Gruber, 2017; Sommaruga et al., 2017).
91 Therefore, there is a common agreement in considering the Jura FTB mainly as the product of thin-
92 skinned tectonics (Sommaruga, 1997). However, thick-skinned tectonics occurred in the late stage
93 of deformation, mostly in the external part (Lacombe and Mouthereau, 2002; Ustaszewski and
94 Schmid, 2006, 2007; Madritsch et al., 2008; Lacombe and Bellahsen, 2016).

95 Field cross-cutting relationships and U-Pb ages of syntectonic calcite mineralizations show
96 that tear faults were synchronously active with thrusting and folding (Sommaruga, 1997; Looser et
97 al., 2021) and their movement continued after thrusting. In fact, in some cases, tear faults are still
98 seismogenic (Thouvenot et al., 1998). Several authors suggested that pre-orogenic strike-slip and
99 normal faults were reactivated in early Pliocene, respectively as tear and transpressional faults
100 (Madritsch et al., 2008; Homberg et al., 1997; Ustaszewski and Schmid, 2006). Overall, direct
101 dating of this fault reactivation is so far not available.

102

103 **3. Methods**

104 The following methods were used: (1) field structural analyses and vein/slickenside sampling
105 from four major thrusts (From SE to NW: Montlebon, Buron, Fuans, and Arguel thrusts) and three
106 NNE-SSW tear faults (Vue des Alpes, Pratz, and Buron) moving from the internal (most deformed)
107 to the external (less deformed) parts of the Jura FTB (Fig. 1). In particular, we measured the
108 orientation of sampled veins and the rake of sampled slickensides in order to combine U-Pb ages
109 from veins and slickensides with structural measurements; (2) microstructural analyses with optical
110 microscope and cathodoluminescence to unravel different phases of calcite precipitation; (3) calcite
111 U-Pb LA-ICP-MS dating on veins and slickensides to date fault activity. In most cases, the U-Pb

112 analyses were performed on calcite crystals showing a homogenous color or undisturbed growth-
113 zoning under cathodoluminescence light, indicating no open-system alteration after calcite
114 precipitation by late fluid infiltration and/or recrystallization (Figs. S1-S3). Analytical details are
115 described in the Supplementary Material.

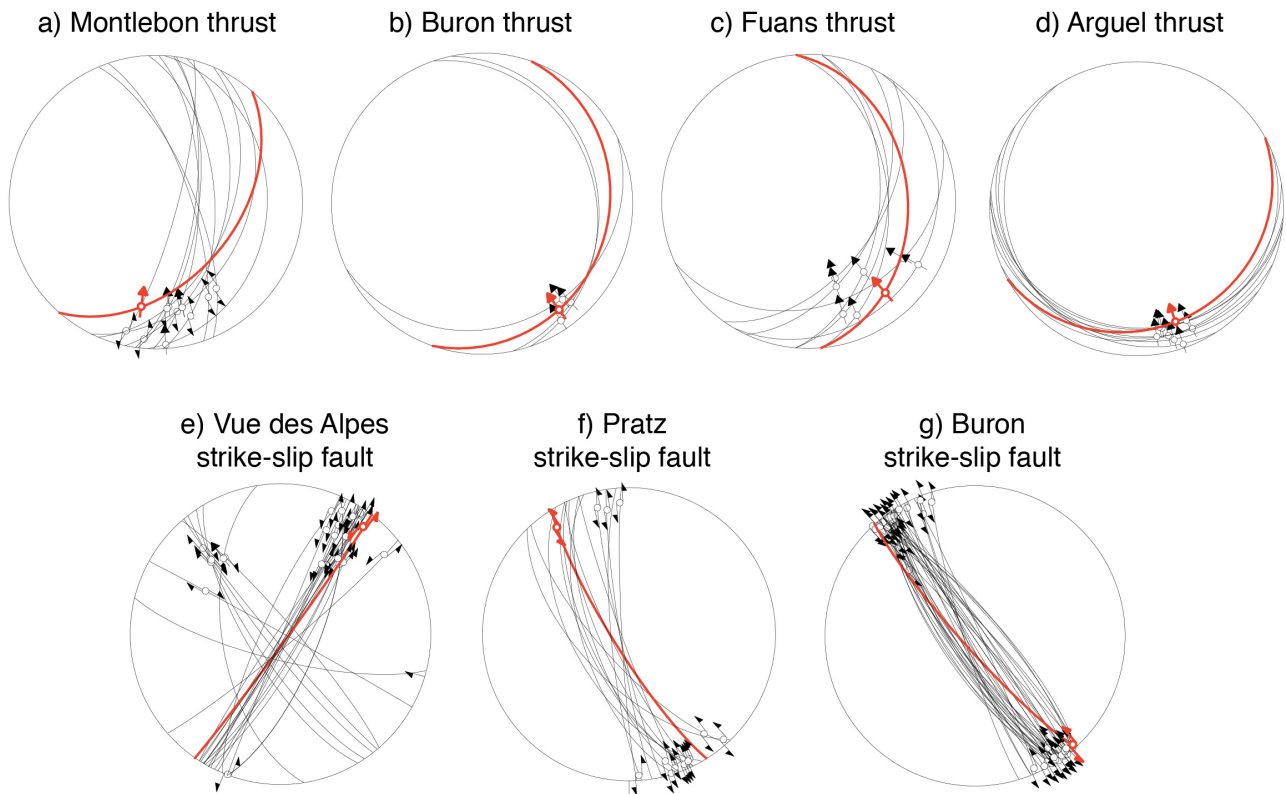
116

117 **4. Results**

118 *4.1 Structural and microstructural observations*

119 The Montlebon, Buron, Fuans, and Arguel thrusts are NNE-SSW- to SW-NE striking and N-
120 to NW-verging thrusts (Madritsch et al., 2008; Rime et al., 2019; Smeraglia et al., 2020) (Fig. 2a-d).
121 More precisely, the Montlebon thrust is characterized by E to ESE-dipping (30-90°) thrust planes
122 with slickenfibers showing left-lateral transpressional movements with N to NNW tectonic
123 transport directions (Fig. 2a). The Buron thrust is characterized by E to SE-dipping (20°-30°) thrust
124 planes with slickenfibers showing left-lateral transpressional movements with NW tectonic
125 transport directions (Fig. 2b). The Fuans thrust is characterized by E to SE-dipping (20°-40°) thrust
126 planes with slickenfibers showing left-lateral transpressional movements with NNW to NW tectonic
127 transport directions (Fig. 2c). The Arguel thrust is characterized by S-dipping (10-30°) thrust planes
128 with slickenfibers showing right-lateral transpressional movements with NNW tectonic transport
129 directions (Fig. 2d).

130 The subvertical Vue des Alpes, Pratz, and Buron tear faults show sinistral strike-slip
131 displacements (Sommaruga, 1997) (Fig. 2de-g). More precisely, the Vue des Alpes strike-slip fault
132 is characterized by NE-SW-striking subvertical fault planes with slickenfibers showing sinistral
133 movements and associated NW-SE-striking subvertical fault planes with slickenfibers showing
134 dextral movements (Fig. 2e). Both the Pratz and Buron strike-slip faults are characterized by NE-
135 SW-striking subvertical fault planes with slickenfibers showing sinistral movements (Fig. 2f-g).



136

137 **Figure 2.** Lower Schmidt hemisphere projection of fault-slip data and slip vectors for thrust and strike-slip faults. Dated
 138 faults in red. **(a)** Montlebon thrust. **(b)** Buron thrust. **(c)** Fuans thrust. **(d)** Arguel thrust. **(e)** Vue des Alpes strike-slip
 139 fault. **(f)** Pratz strike-slip fault. **(g)** Buron strike-slip fault-

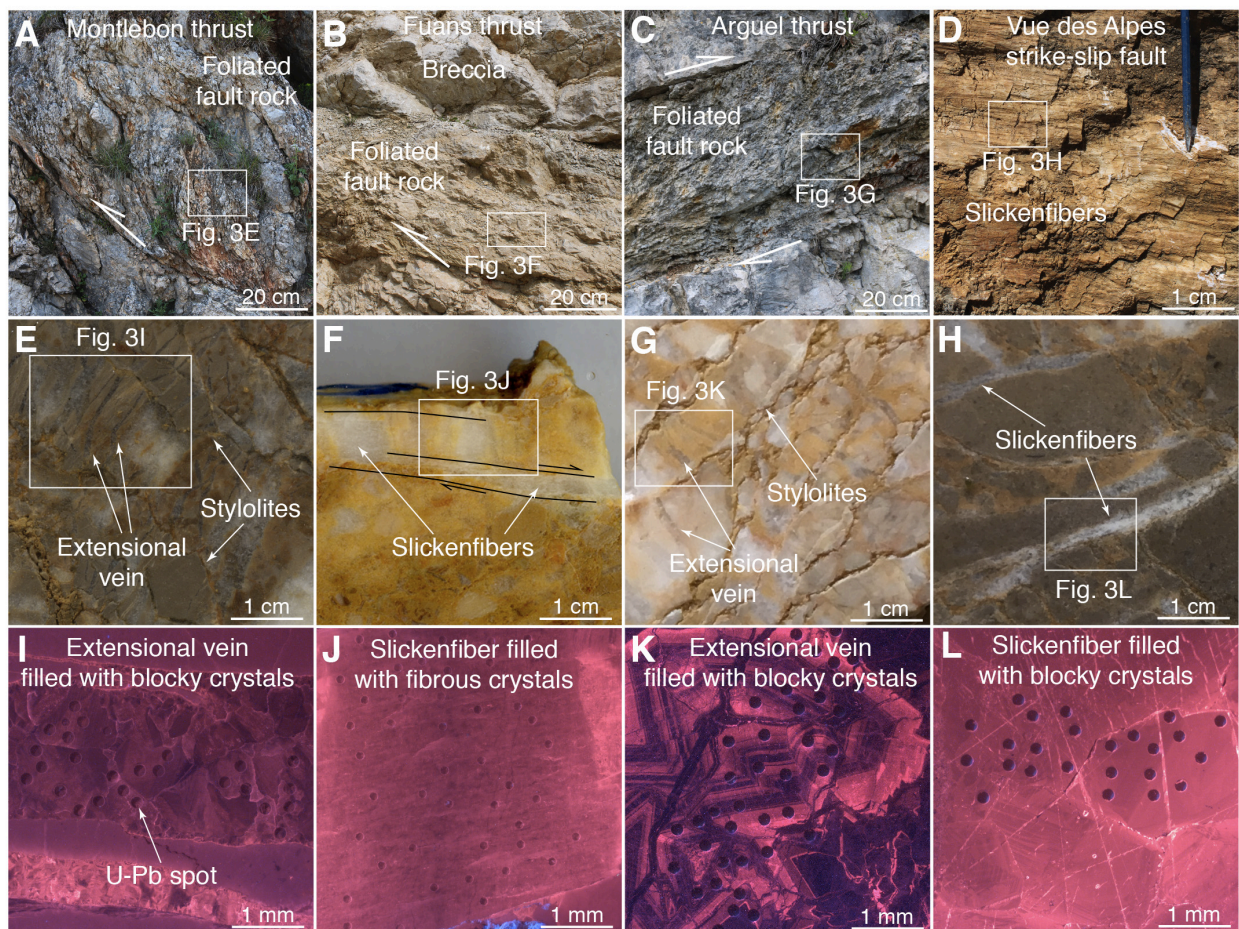
140

141 Both thrusts and strike-slip faults cut through Middle-Upper Jurassic and Lower Cretaceous
 142 limestones. The fault core zones are characterized by foliated fault rocks cut by sharp fault planes
 143 (Fig. 3a-d). Breccia lenses are developed in the Buron thrust core (Fig. 4d). Calcite mineralizations
 144 in extensional veins (Buron, Arguel, Montlebon, Vue des Alpes, and Pratz) and in slickenfibers
 145 (Fuans, Vue des Alpes, and Pratz) were sampled.

146 Extensional veins occur in limestone fragments of foliated fault rocks (Fig. 3e,g) and in clasts
 147 from breccias (Figs. 3f and 4g). In limestone fragments of foliated fault rocks, extensional veins are
 148 oriented perpendicularly to stylolites (Fig. 3e,g), which occur along S- and C-planes. Extensional
 149 veins in clasts from breccias show a crackle-like texture and mutually cross-cutting relationships
 150 (Fig. 3f). Extensional veins are filled by blocky to elongated-blocky calcite crystals and show
 151 syntaxial growth (Figs. 3i-k, 4g, S1a-d, S2a,b,g,h, S3a-h).

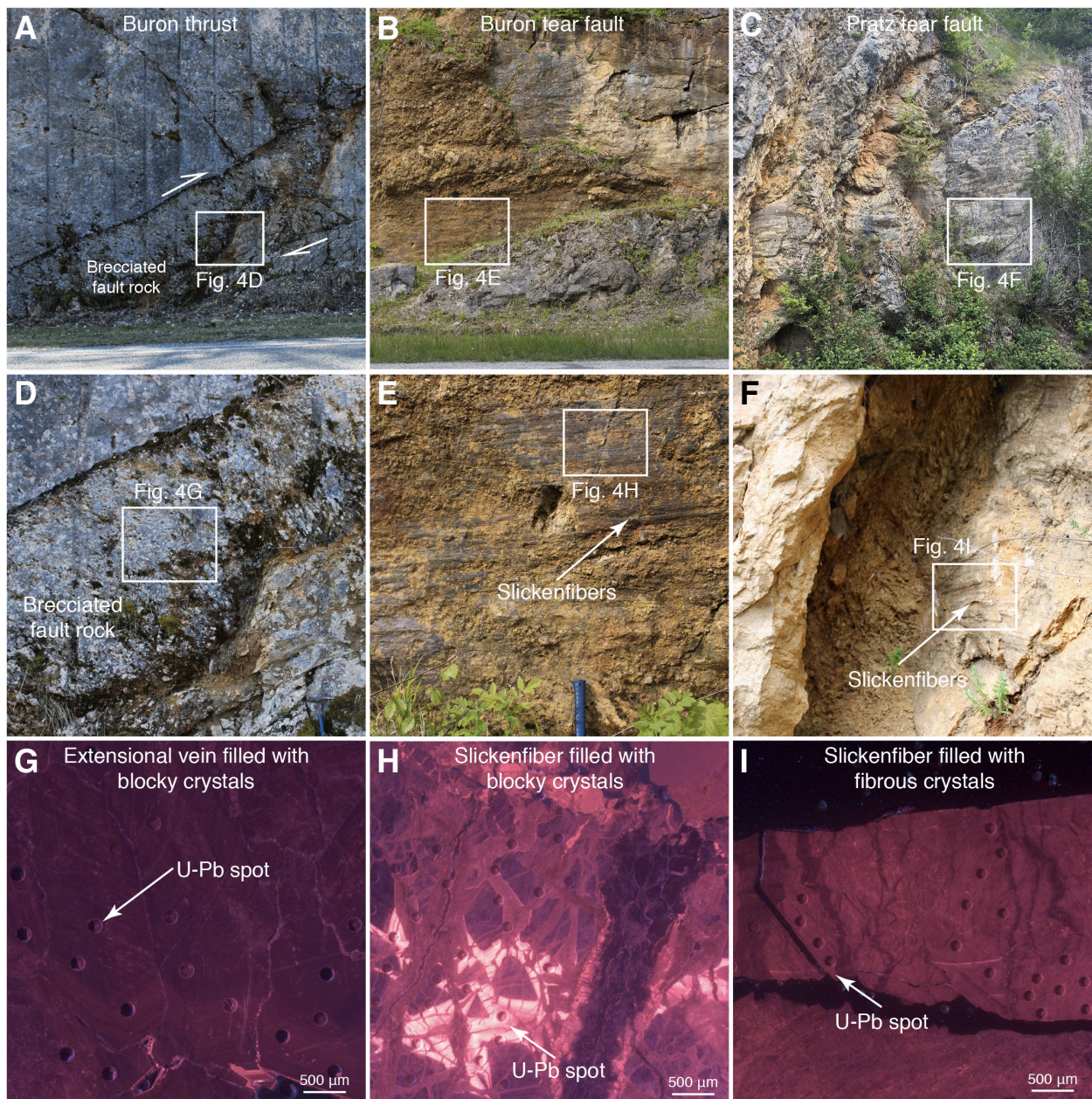
152 The fault planes are coated by slickenfibers (Figs. 3d,h and 4e,f). At the microscale,
 153 slickenfibers occur in dilational jogs along shear planes (Fig. 3h) and are filled by fibrous calcite
 154 crystals bounded by sharp shear planes (Figs. 3j, 4i, S1e-h, and S2c-f) and/or by blocky calcite
 155 crystals (Figs. 3l and 4h). Fibrous crystals are oriented parallel to shear planes.

156 Most of the studied veins and slickenfibers show homogeneous cathodoluminescence colors,
 157 ranging from bright to dull red, and/or show cathodoluminescence zoning on the same crystal (Figs.
 158 3i-l, 4g-i, S1a,c,e,g, S2a,c,e,g, and S3a,c,e,g). In places, slickenfibers and extensional veins are
 159 cross-cut by extensional veins showing black to dull red luminescence colors (Figs. S1e-h, S2c-f,
 160 and S3a,b,g,h)



161
 162 **Figure 3.** Foliated fault rocks in the fault core of the Montlebon thrust (a), Arguel thrust (b), and (c) Fuans thrust. (d)
 163 Detail of minor fault plane along the Vue des Alpes strike-slip fault showing calcite slickenfibers. (e) Hand sample from
 164 the Montlebon thrust showing host rock sigmoids bounded by stylolites and extensional veins perpendicular to
 165 stylolites. (f) Hand sample from the Fuans thrust showing host rock sigmoids bounded by stylolites and extensional

166 veins perpendicular to stylolites. **(g)** Hand sample from the Arguel thrust showing extensional veins with crackle-like
 167 texture. **(h)** Hand sample from a minor fault plane along the Vue des Alpes strike-slip fault showing slickenfibers
 168 developed along dissolution planes. **(i-l)** Cathodoluminescence microphotographs of thin sections showing extensional
 169 veins and slickenfibers from the studied faults with ablation craters of the U-Pb analyses.
 170



171
 172 **Figure 4.** **(a)** Buron thrust. **(b)** Buron tear fault. **(c)** Pratz tear fault. **(d)** Brecciated fault rocks in the fault core of the
 173 Buron thrust. **(e)** Brecciated fault rocks cut by sharp fault planes in the fault core of the Buron tear fault. **(f)** Foliated
 174 fault rock cut by sharp fault planes in the fault core of the Pratz tear fault. **(g-i)** Cathodoluminescence microphotographs

175 of thin sections showing extensional veins and slickenfibers from the studied faults with ablation craters of the U-Pb
176 analyses.

177

178 4.2 U-Pb dating

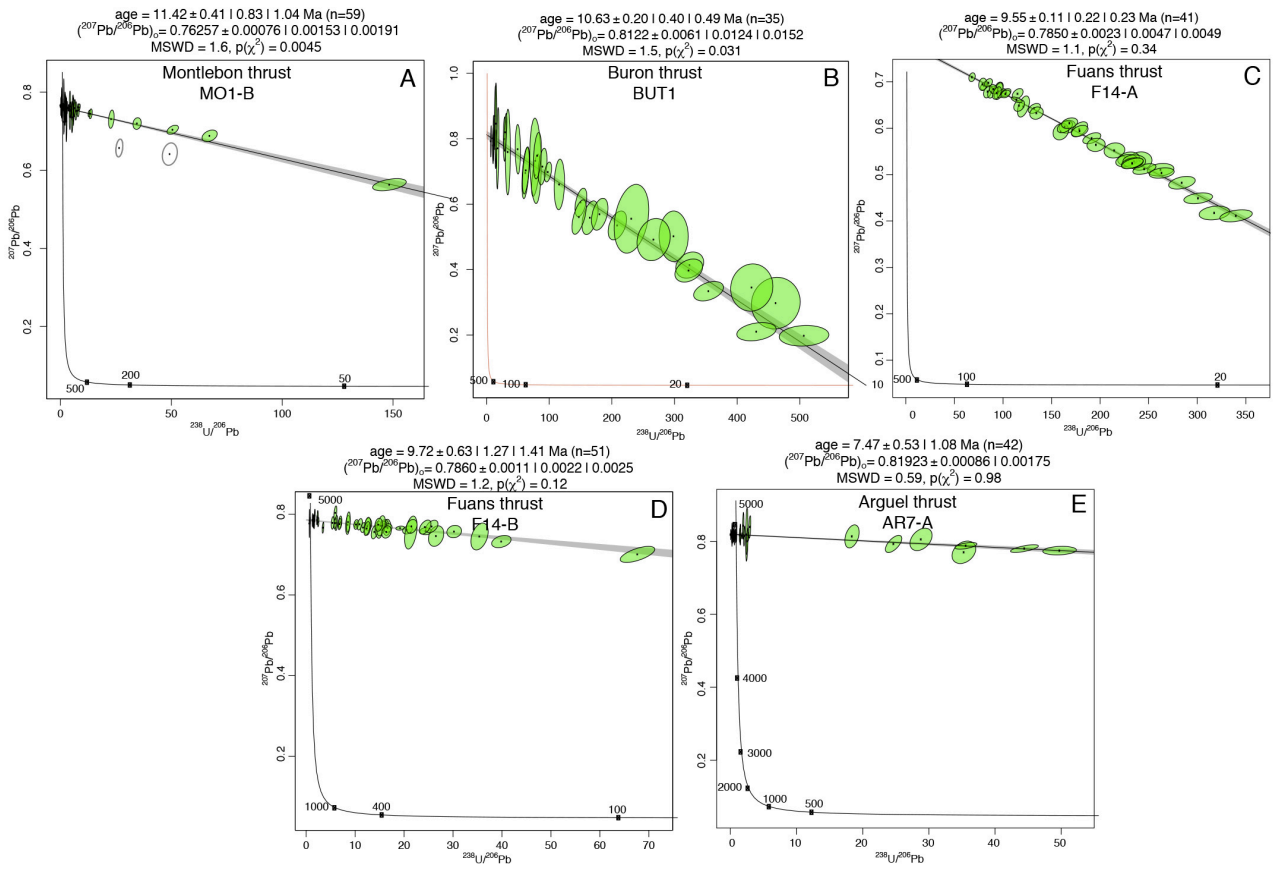
179 A total of 12 reliable lower intercept ages (Figs. 5 and 6) out of 19 analyses (rejected age data
180 is presented in Fig. S4) are reported with uncertainties at 2σ absolute including counting statistics
181 uncertainties, uncertainty of the primary reference material and inter-session variations (Guillong et
182 al., 2020). The U-Pb ages indicate different phases of tectonic activity and related calcite
183 precipitation in the middle Eocene to Pliocene period and also multiple precipitation ages along the
184 same fault (Supplementary Information Table 1).

185 An extensional vein from the Montlebon thrust shows a Serravallian age of 11.4 ± 1.1 Ma
186 (Fig. 5a). An extensional vein from the Buron thrust shows a Tortonian age of 10.6 ± 0.5 Ma (Fig.
187 5b). Two slickenfibers from the Fuans thrust yield Tortonian ages indistinguishable from each other
188 of 9.7 ± 1.4 Ma and 9.6 ± 0.3 , respectively (Fig. 5c,d). An extensional vein from the Arguel thrust
189 shows a Tortonian-Messinian age of 7.5 ± 1.1 Ma (Fig. 5e). Along the Vue des Alpes strike-slip
190 fault, two slickenfibers yield Ypresian-Lutetian ages of 44.7 ± 2.6 and 48.4 ± 1.5 Ma (Fig. 6a,b),
191 while an extensional vein shows a Pliocene age of 3.9 ± 2.9 Ma (Fig. 6c). An extensional vein from
192 the Buron strike-slip fault shows a Messinian age of 5.7 ± 4.7 Ma (Fig. 6d). One slickenfiber and
193 one extensional vein from the Pratz strike-slip fault show Tortonian-Messinian ages of 10.5 ± 0.4
194 and 9.1 ± 6.5 Ma (Fig. 6f-g), while one slickenfiber shows a younger age of 4.8 ± 1.7 Ma (Fig. 6e).
195 Because of the common-lead rich $^{207}\text{Pb}/^{206}\text{Pb}$ compositions, the U-Pb ages of the samples DA2,
196 BUS1, PR1-A, PR2-2 of the strike-slip faults have larger uncertainties than those of the thrusts.

197

198

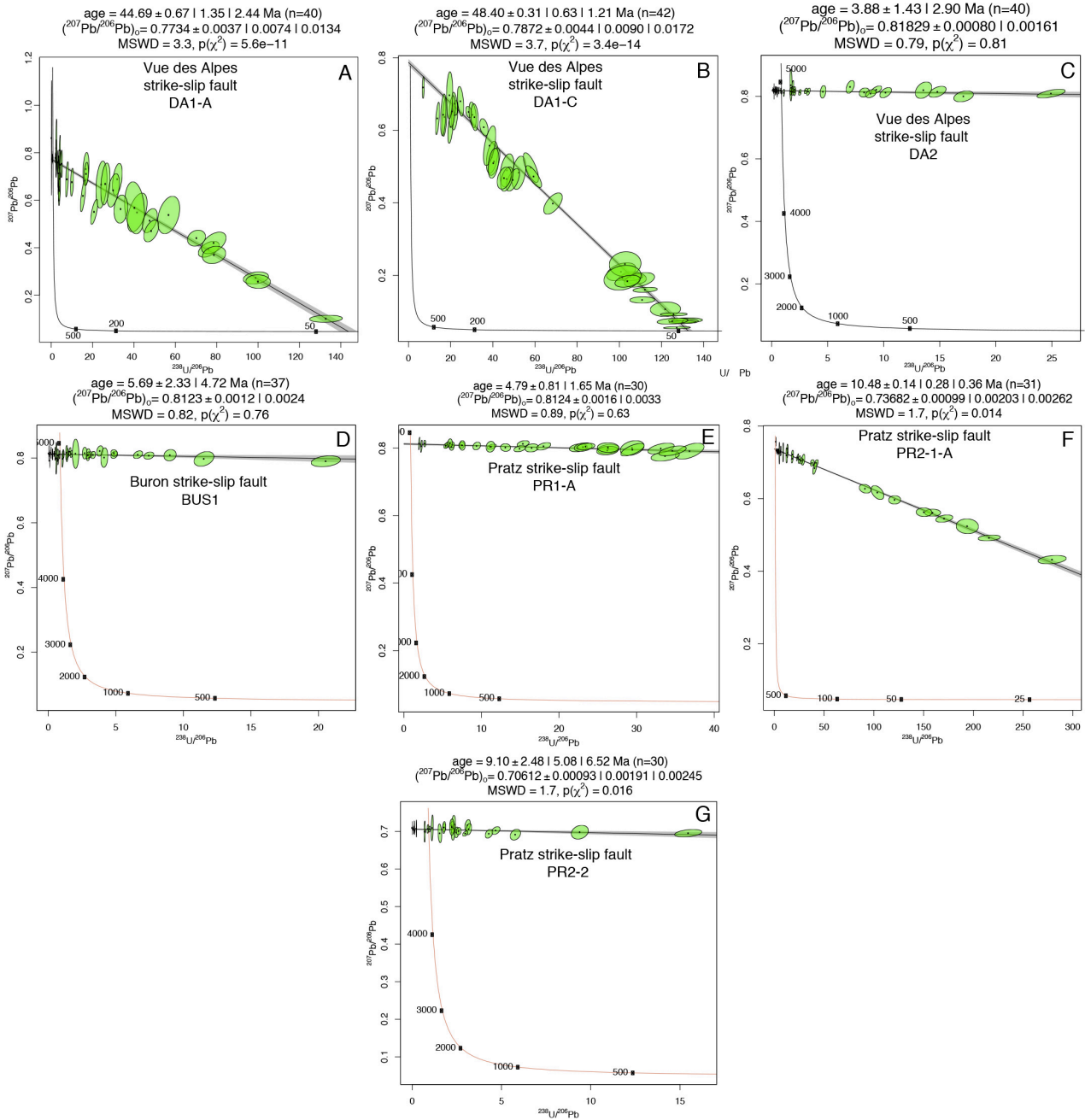
U-Pb ages from thrusts



199

200 **Figure 5.** Tera-Wasserburg concordia diagrams of thrust faults. **(a)** Montlebon thrust. **(a)** Buron thrust. **(c,d)** Fuans
 201 thrust. **(e)** Arguel thrust.

U-Pb ages from strike-slip faults



202

203 **Figure 6.** Tera-Wasserburg concordia diagrams of strike-slip faults. **(a-c)** Vue des Alpes strike-slip fault. **(d)** Buron
 204 strike-slip fault. **(e-g)** Pratz strike-slip fault.

205

206 5. Discussion and conclusions

207 Slickenfibers on sharp fault planes are clear evidence of tectonic slip along faults (Figs. 3j-l,

208 4i, S1e-h, and S2c,f). In particular, blocky and fibrous crystals indicate respectively fast and slow

209 vein opening rates associated with fault slip. Within slickenfibers, calcite crystal precipitated during
210 syn- to early post-slip fluid influx in newly formed dilational sites formed along undulated and
211 sharp slip planes (Gratier and Gamond, 1990; Urai et al., 1991; Holland and Urai, 2010; Fagereng et
212 al., 2010; Bons et al., 2012; Woodcock et al., 2014). Extensional veins oriented perpendicular to
213 stylolites (Fig. 3e,g) are linked to syn-thrusting shortening (Gratier et al., 2013). The studied veins
214 are therefore interpreted as the product of tectonic fault slip and their U-Pb ages are considered as
215 representative of faulting activity.

216 We recognize three regional tectonic phases between the middle Eocene and the Pliocene
217 (Figs. 7 and 8), which are linked to the long-lived tectonic activity of the Alpine foreland evolution.
218 The presented ages should be regarded as minimum ages for the onset of deformation at the studied
219 faults or as maximum ages for its termination as potentially older or younger deformation phases
220 recorded by other veins and slickenfibers not sampled and analyzed here may have been missed. As
221 commonly done in carbonate LA-ICP-MS U-Pb dating, no disequilibrium correction for initial
222 $^{234}\text{U}/^{238}\text{U}$ and ^{230}Th was applied. This may cause underestimation of young (<10 Ma) samples
223 (Roberts et al. 2020) and accordingly, they should be regarded to reflect maximal ages.

224 The U-Pb ages are regionally consistent in terms of the tectonic evolution of the Jura FTB,
225 and the microstructures of the analyzed veins and slickenfibers indicate precipitation during syn- to
226 early post-slip fluid influx. However, although U-Pb dating was performed on crystals with no
227 indication of later open-system alteration based on CL-microscopy, possible late fluid infiltration
228 and calcite recrystallization cannot be excluded as previously suggested by other studies (Beaudoin
229 et al., 2018; Hoareau et al., 2021; Roberts et al., 2020, 2021).

230 Sample BUS1 clearly shows multiple calcite phases indicating vein re-opening and
231 potentially different ages (Fig. 4h). However, the Tera-Wasserburg diagram of BUS1 shows a
232 single age trend with a low MSWD of 0.82 (Fig. 6d). This would not be observed in a sample that
233 experienced crystallization at significantly different times. Therefore, sample BUS1 reflects calcite
234 precipitation within a time interval smaller than what would result in multiple age trends.

235 The oldest tectonic phase is recorded by two horizontal slickenfibers dated at 44.7 ± 2.6 and
236 48.4 ± 1.5 Ma in Ypresian-Lutetian times (middle Eocene) along the Vue des Alpes strike-slip fault
237 (Fig. 7). These ages are ~ 10 Ma older than the onset of the extensional tectonic activity in
238 Priabonian (late Eocene) related to Rhine Graben opening (Sissingh, 1998; Mazurek et al. 2018).
239 The strike-slip faulting in Eocene times is consistent with fault-slip data of Homberg et al. (1997).
240 We propose that the Ypresian-Lutetian tectonic activity can be related to the late Mesozoic-Eocene
241 far field tectonic shortening in the European plate foreland due to the advancing Alpine orogen
242 (Mazurek et al., 2006; Timar-Geng et al., 2006) (Fig. 8a). However, previous studies suggested that
243 middle Eocene strike-slip faulting in the Jura area can be also related to the far-field effect of the
244 Pyrenean compression (Bergerat, 1987; Homberg et al., 2002). The Pyrenean far field effect is also
245 recognized in the Paris Basin (e.g., Lacombe et al., 1990; Lacombe and Mouthereau, 1999;
246 Lacombe and Obert, 2000), in eastern France (Lacombe et al., 1993), and even in the United
247 Kingdom (Hibsch et al., 1995) where Pyrenean-related calcite veins were dated by U-Pb (ages
248 between 55 and 25 Ma; Parrish et al., 2018). Therefore, we cannot fully distinguish if the strike-slip
249 fault activity during Ypresian-Lutetian times is related to the Pyrenean or to the Alpine shortening.
250 Further studies are necessary to better constrain the origin of pre-Miocene fault activity in the
251 European foreland.

252 Structural analyses of the studied thrusts highlight N to NW oriented tectonic transport
253 directions (Fig. 4a-d) consistent with the regional NW-SE to N-S compressional phase that has
254 affected the Jura fold and thrust belt since the Miocene (Philippe et al, 1996; Becker, 2000;
255 Homberg et al., 2002; Ustaszewski and Schmid, 2006; Madritsch et al., 2008; Looser et al., 2021).
256 Although age uncertainties do not allow a distinction beyond doubt and the limited numbers of U-
257 Pb ages and studied thrusts provide a limited picture, the Jura imbrication seems to have occurred
258 by in-sequence thrusting. The oldest observed thrusts ages are Serravallian-Messinian and become
259 progressively younger moving from the inner (SE) toward the external (NW) part, from 11.4 ± 1.1 ,
260 10.6 ± 0.5 , 9.7 ± 1.4 and 9.6 ± 0.3 on the same thrust, and 7.5 ± 1.1 Ma, respectively, in the

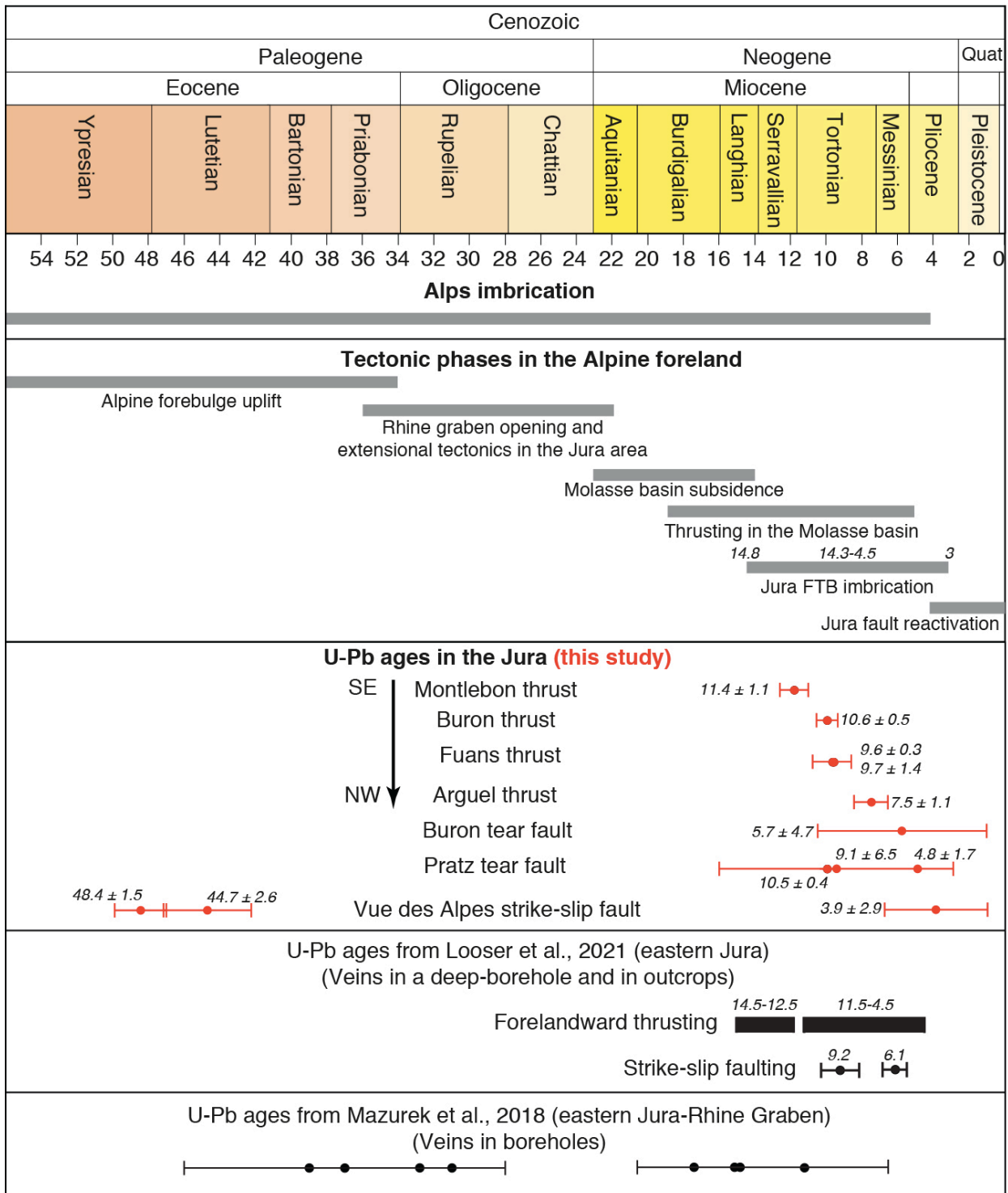
261 Montlebon, Buron, Fuans, and Arguel thrusts (Figs. 7 and 8b). These ages are consistent with the
262 time interval of ~ 14.5 - 3.3 Ma suggested for thrusting activity from biostratigraphic dating of syn- to
263 post-tectonic sediments (Becker, 2000 and references therein) and from calcite U-Pb ages of thrust
264 activity in the eastern Jura FTB (Looser et al., 2021) (Fig. 7).

265 Previous studies interpreted the subvertical strike-slip faults in the Jura FTB as tear faults,
266 with activity during thrusting and folding (Sommaruga, 1997; Looser et al., 2021). Our structural
267 analyses and U-Pb ages from the studied strike-slip faults support this interpretation. In particular,
268 strike-slip faults are subvertical and are roughly parallel or oblique to the regional transport
269 directions inferred from thrust kinematics (compare tectonic transport directions of Fig. 4a-d with
270 those of Fig. 4f,g), a common feature of tear faults (Twiss and Moores, 1992).

271 The Buron thrust, active at 10.6 ± 0.5 Ma, was cross-cut by the Buron tear fault ~ 5 Ma later,
272 at 5.7 ± 4.7 Ma (Figs. 7 and 8c). The Pratz tear fault was active at 10.5 ± 0.4 and 9.1 ± 6.5 Ma,
273 indicating tear faulting generation during coeval thrust propagation, and further late-orogenic re-
274 activation at 4.8 ± 1.7 Ma (Figs. 7 and 8b). These data indicate that tear faulting occurred during
275 syn- to late-orogenic times (Fig. 8b,c). In addition, a late-orogenic phase is recorded by an
276 extensional vein from the Vue des Alpes strike-slip fault showing a Pliocene age of 3.9 ± 2.9 Ma
277 (Fig. 7). This age has been measured on an extensional vein that cannot be directly related to fault
278 slip. Therefore, we cannot completely exclude that this age represents a late alteration event not
279 directly linked to fault slip during the Pliocene. However, the 3.9 ± 2.9 Ma age is consistent with
280 late orogenic deformation between 4.2 and 2.9 Ma documented in the frontal part of the Jura FTB
281 (Madritsch et al., 2008 and references therein). The 3.9 ± 2.9 Ma age from the Vue des Alpes strike-
282 slip fault is ~ 40 Ma younger than the middle Eocene ages (44.7 ± 2.6 and 48.4 ± 1.5 Ma) measured
283 on the same fault, suggesting the reactivation of the Vue des Alpes strike-slip fault during late Jura
284 shortening. This inference is also consistent with field cross-cutting relationships indicating re-
285 activation of pre-existing strike-slip faults as tear faults (Homberg et al., 1997).

286 We consider the retrieved age as fault re-activation of the Vue des Alpes strike-slip fault and
287 relate it to a stress change from pure compression to strike-slip state of stress coupled with the
288 occurrence of an inherited strike-slip fault favorably oriented with respect to the regional stress
289 field. This stress change associated with tear fault development can be related to progressive fold-
290 and-thrust belt thickening initiating only after ~4.5 Ma (Looser et al., 2021 and references therein),
291 which led to an increase in the principal vertical stress (σ_3) and a switch between σ_3 and
292 σ_2 (Ferril et al., 2021). Shortening is still active in the Jura FTB and tear faults (also re-
293 activated tear faults) are seismogenic (Thouvenot et al., 1998).

294 The presented tectonic reconstruction depicts a stable evolution of the Jura FTB wedge by
295 possible in-sequence thrusting consistent with thrust imbrication above the low-friction décollement
296 consisting of evaporites (Fig. 8a-c). Contrarily, out-of-sequence thrusting occurred as late as in
297 Messinian-early Pliocene times in the proximal Molasse Basin (Von Hagke et al., 2012, 2014) and
298 in the Alps (Bellahsen et al., 2014). This tectonic framework suggests a stable topographic
299 evolution of the critical taper and topographic profile of the Jura fold-and-thrust belt. Finally, this
300 study constrains a long-lived polyphase tectonic history of the northwestern Alpine foreland system
301 along the convergent boundary between European and African plates from the middle Eocene to the
302 Pliocene.



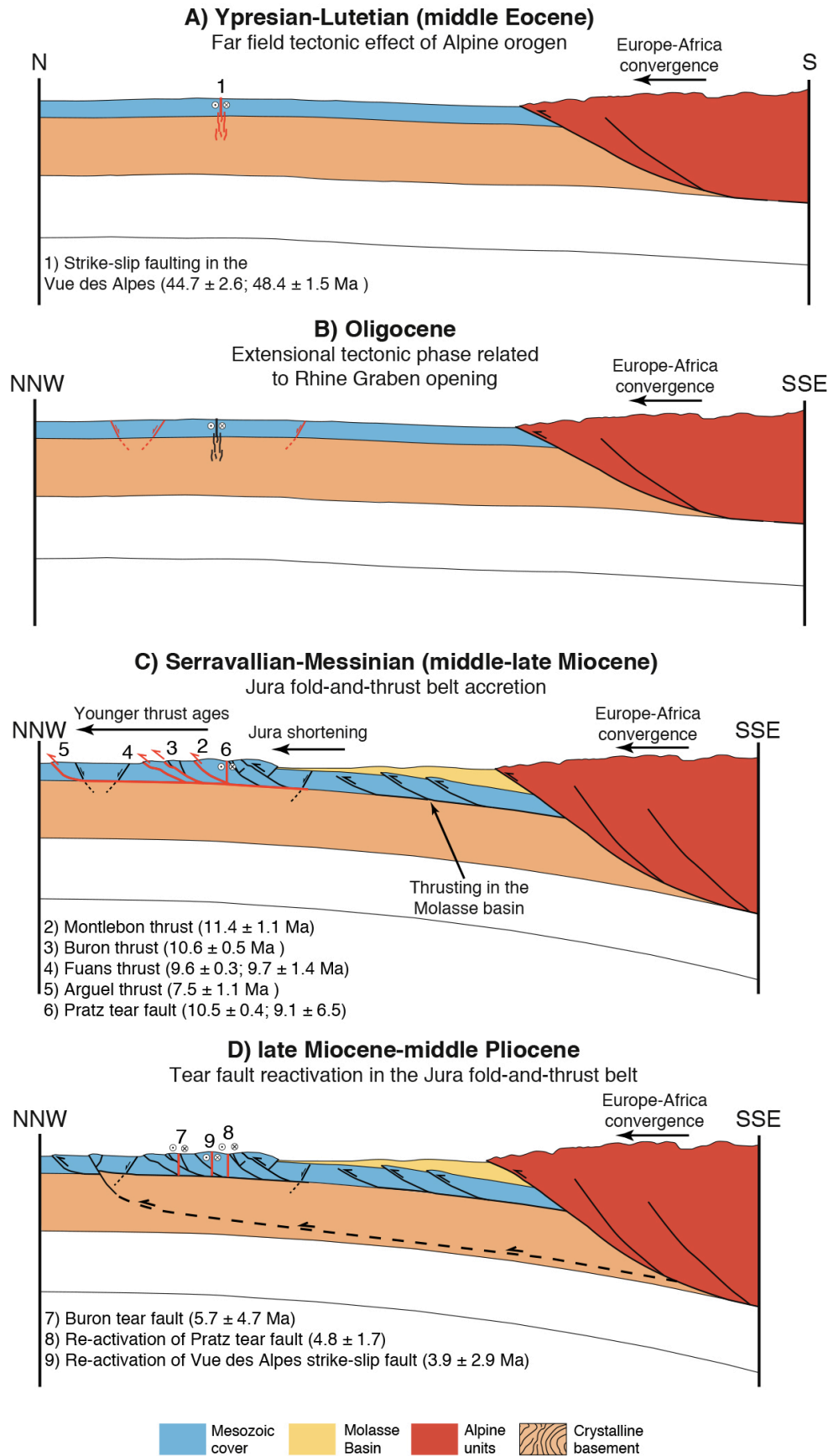
303

304

305

306

Figure 7. Main tectonic phases in the Alps and in the Alpine foreland. Age constraints shown as grey bars are from Burkhard and Sommaruga (1998), Ustaszewski et al. (2006), Madritsch et al. (2008), Bellahsen et al. (2014), and Von Hagke et al. (2014). For calcite U-Pb data, all uncertainties are represented as 2σ .



307

308 **Figure 8. (a-d)** Schematic reconstruction of the main tectonic phases dated in the Jura area in the regional context of the

309 Alpine foreland system evolution.

310 **ACKNOWLEDGEMENT**

311 We thank CASP (<https://www.casp.org.uk/>) for financial support during fieldwork activity by
312 the Andy Whitham Fieldwork Award 2019 to L. Smeraglia. Financial support by Borsa di
313 Perfezionamento Estero 2017 (Sapienza) to L. Smeraglia, UMR 6249 and OSU Theta projects to O.
314 Fabbri and F. Choulet are acknowledged. U-Pb analyses were funded by the Swiss National Science
315 Foundation project number 200021_169849 to S. M. Bernasconi. We thank J. Mosar, M. Schori, A.
316 Sommaruga, C. Mottran, L. Weiss, and C. Von Hagke for constructive discussions and suggestions,
317 also during fieldwork. We thank the Editor Susanne Buiter and two reviewers Olivier Lacombe and
318 Nick Roberts for their constructive comments that helped to improve the manuscript.

319

320 **REFERENCES**

- 321 Affolter, T., and Gratier, J. P.: Map view retrodeformation of an arcuate fold-and-thrust belt: The
322 Jura case. *Journal of Geophysical Research: Solid Earth*, 109(B3), 2004.
- 323 Beaudoin, N., and Lacombe, O.: Recent and future trends in paleopiezometry in the diagenetic
324 domain: Insights into the tectonic paleostress and burial depth history of fold-and-thrust belts
325 and sedimentary basins. *Journal of Structural Geology*, 114, 357-365, 2018.
- 326 Beaudoin, N., Leprêtre, R., Bellahsen, N., Lacombe, O., Amrouch, K., et al.: Structural and
327 microstructural evolution of the Rattlesnake Mountain Anticline (Wyoming, USA): new
328 insights into the Sevier and Laramide orogenic stress build-up in the Bighorn Basin.
329 *Tectonophysics*, 576, 20-45, 2012.
- 330 Beaudoin, N., Lacombe, O., Roberts, N. M., and Koehn, D.: U-Pb dating of calcite veins reveals
331 complex stress evolution and thrust sequence in the Bighorn Basin, Wyoming, USA.
332 *Geology*, 46(11), 1015-1018, 2018.
- 333 Becker, A.: The Jura Mountains - an active foreland fold-and-thrust belt?. *Tectonophysics*, 321(4),
334 381-406, 2000.

335 Bellahsen, N., Mouthereau, F., Boutoux, A., Bellanger, M., Lacombe, O., Jolivet, L., and Rolland,
336 Y. : Collision kinematics in the western external Alps. *Tectonics*, 33(6), 1055-1088, 2014.

337 Bergerat, F.: Stress fields in the European platform at the time of Africa-Eurasia collision.
338 *Tectonics* 6, 99-132, 1987.

339 Bons, P. D., Elburg, M. A., and Gomez-Rivas, E.: A review of the formation of tectonic veins and
340 their microstructures. *Journal of Structural Geology*, 43, 33-62, 2012.

341 Carminati E., Aldega L., Smeraglia L., Scharf A., Mattern F., Albert R., and Gerdes A.: Tectonic
342 evolution of the Northern Oman Mountains, part of the Strait of Hormuz Syntaxis: new
343 structural and paleothermal analyses and U-Pb dating of synkinematic calcite. *Tectonics* 39,
344 e2019TC005936, 2020.

345 Craig, M. S., and Warvakai, K.: Structure of an active foreland fold and thrust belt, Papua New
346 Guinea. *Australian Journal of Earth Sciences*, 56(5), 719-738, 2009.

347 Craddock, J. P., Jackson, M., van der Pluijm, B. A., & Versical, R. T.: Regional shortening fabrics
348 in eastern North America: Far-field stress transmission from the Appalachian-Ouachita
349 Orogenic Belt. *Tectonics*, 12(1), 257-264, 1993.

350 Fagereng, Å., Remitti, F., and Sibson, R. H.: Shear veins observed within anisotropic fabric at high
351 angles to the maximum compressive stress. *Nature Geoscience*, 3(7), 482, 2010.

352 Ferril, D.A., Smart, K.J., Cawood, A.J., Morris, A.P.: The fold-thrust belt stress cycle:
353 Superposition of normal, strike-slip, and thrust faulting deformation regimes. *Journal of*
354 *Structural Geology* 148, 104362, 2021.

355 Goodfellow, B. W., Viola, G., Bingen, B., Nuriel, P., and Kylander-Clark, A. R.: Paleocene faulting
356 in SE Sweden from U–Pb dating of slickenfiber calcite. *Terra Nova*, 29(5), 321-328, 2017.

357 Gratier, J. P., and Gamond, J. F.: Transition between seismic and aseismic deformation in the upper
358 crust. *Geological Society, London, Special Publications*, 54(1), 461-473, 1990.

359 Gratier, J.P., Thouvenot, F., Jenatton, L., Tourette, A., Doan, M.L., Renard, F.: Geological control
360 of the partitioning between seismic and aseismic sliding behaviours in active faults: evidence
361 from the Western Alps, France. *Tectonophysics* 600, 226-242, 2013.

362 Gruber, M.: Structural Investigations of the Western Swiss Molasse Basin - From 2D Seismic
363 Interpretation to a 3D Geological Model. *GeoFocus*, 41, 190 pp, 2017.

364 Guillong, M., Wotzlaw, J., Looser, N., & Laurent, O. (2020). Evaluating the reliability of U–Pb
365 laser ablation inductively coupled plasma mass spectrometry (LA-ICP-MS) carbonate
366 geochronology: Matrix issues and a potential calcite validation reference material.
367 *Geochronology*, 2, 155–167. <https://doi.org/10.5194/gchron-2-155-2020>.

368 Hansman, R. J., Albert, R., Gerdes, A., and Ring, U.: Absolute ages of multiple generations of
369 brittle structures by U-Pb dating of calcite. *Geology*, 46(3), 207-210, 2018.

370 Hibschi, C., Jarrige, J. J., Cushing, E. M., and Mercier, J.: Palaeostress analysis, a contribution to the
371 understanding of basin tectonics and geodynamic evolution. Example of the
372 Permian/Cenozoic tectonics of Great Britain and geodynamic implications in western Europe.
373 *Tectonophysics*, 252(1-4), 103-136, 1995.

374 Hoareau, G., Crognier, N., Lacroix, B., Aubourg, C., Roberts, N. M., et al.: Combination of $\Delta 47$
375 and U-Pb dating in tectonic calcite veins unravel the last pulses related to the Pyrenean
376 Shortening (Spain). *Earth and Planetary Science Letters*, 553, 116636, 2021.

377 Holland, M., and Urai, J. L.: Evolution of anastomosing crack–seal vein networks in limestones:
378 Insight from an exhumed high-pressure cell, Jabal Shams, Oman Mountains. *Journal of*
379 *Structural Geology*, 32(9), 1279-1290, 2010.

380 Homberg, C., Hu, J. C., Angelier, J., Bergerat, F., and Lacombe, O.: Characterization of stress
381 perturbations near major fault zones: insights from 2-D distinct-element numerical modelling
382 and field studies (Jura mountains). *Journal of Structural Geology*, 19(5), 703-718, 1997.

383 Homberg, C., Bergerat, F., Philippe, Y., Lacombe, O., and Angelier, J.: Structural inheritance and
384 Cenozoic stress fields in the Jura fold-and-thrust belt (France). *Tectonophysics*, 357(1-4),
385 137-158, 2002.

386 Jordan, P.: Evidence for large-scale decoupling in the Triassic evaporites of Northern Switzerland:
387 an overview. *Eclogae Geologicae Helvetiae*, 85, 677–693, 1992.

388 Lacombe, O., Angelier, J., Laurent, P., Bergerat, F., and Tournéret, C.: Joint analyses of calcite
389 twins and fault slips as a key for deciphering polyphase tectonics: Burgundy as a case study.
390 *Tectonophysics*, 182(3-4), 279-300, 1990.

391 Lacombe, O., Angelier, J., Byrne, D., and Dupin, J. M.: Eocene-Oligocene tectonics and kinematics
392 of the Rhine-Saone continental transform zone (eastern France). *Tectonics*, 12(4), 874-888,
393 1993.

394 Lacombe, O., and Mouthereau, F.: What is the real front of orogens? The Pyrenean orogen as a case
395 study. *Comptes Rendus de l'Académie des Sciences Series IIA Earth and Planetary Science*,
396 329(12), 889-896, 1999.

397 Lacombe, O., & Mouthereau, F. (2002). Basement-involved shortening and deep detachment
398 tectonics in forelands of orogens: Insights from recent collision belts (Taiwan, Western Alps,
399 Pyrenees). *Tectonics*, 21(4), 12-1.

400 Lacombe, O., and Obert, D.: Structural inheritance and cover deformation: Tertiary folding and
401 faulting in, the western Paris Basin. *Comptes rendus de l'academie des sciences serie ii*
402 *fascicule a-sciences de la terre et des planetes*, 330(11), 793-798, 2000.

403 Lacombe, O., Lavé, J., Roure, F. M., and Vergés, J. (Eds.): Thrust belts and foreland basins: From
404 fold kinematics to hydrocarbon systems. Springer Science & Business Media, 2007.

405 Lacombe, O., and Bellahsen, N.: Thick-skinned tectonics and basement-involved fold–thrust belts:
406 insights from selected Cenozoic orogens. *Geological Magazine*, 153, 763-810, 2016.

407 Looser, N., Madritsch, H., Guillong, M., Laurent, O., Wohlwend, S., & Bernasconi, S. M. (2021).
408 Absolute age and temperature constraints on deformation along the basal décollement of the

409 Jura fold-and- thrust belt from carbonate U-Pb dating and clumped isotopes. *Tectonics*, 40,
410 e2020TC006439. <https://doi.org/10.1029/2020TC006439>

411 Madritsch, H., Schmid, S. M., and Fabbri, O.: Interactions between thin- and thick-skinned
412 tectonics at the northwestern front of the Jura fold-and-thrust belt (eastern France). *Tectonics*,
413 27, 1-31, 2008.

414 Mazurek, M., Davis, D. W., Madritsch, H., Rufner, D., Villa, I. et al. (2018). Veins in clay-rich
415 aquitards as records of deformation and fluid-flow events in northern Switzerland. *Applied*
416 *Geochemistry*, 95, 57-70, 2008.

417 Mazurek, M., Hurford, A. J., and Leu, W.: Unravelling the multi-stage burial history of the Swiss
418 Molasse Basin: integration of apatite fission track, vitrinite reflectance and biomarker
419 isomerisation analysis. *Basin Research*, 18, 27–50, 2006.

420 Merle, O., & Michon, L. (2001). The formation of the West European Rift; a new model as
421 exemplified by the Massif Central area. *Bulletin de la Societé géologique de France*, 172(2),
422 213-221.

423 Mosar, J.: Present-day and future tectonic underplating in the western Swiss Alps: reconciliation of
424 basement/wrench-faulting and décollement folding of the Jura and Molasse basin in the
425 Alpine foreland. *Earth and Planetary Science Letters*, 173, 143-155, 1999.

426 Nuriel, P., Weinberger, R., Kylander-Clark, A. R. C., Hacker, B. R., and Craddock, J. P.: The onset
427 of the Dead Sea transform based on calcite age-strain analyses. *Geology*, 45(7), 587-590,
428 2017.

429 Parrish, R. R., Parrish, C. M., and Lasalle, S.: Vein calcite dating reveals Pyrenean orogen as cause
430 of Paleogene deformation in southern England. *Journal of the Geological Society*, 175(3),
431 425-442, 2018.

432 Philippe, Y., Colletta, B., Deville, E., and Mascle, A.: The Jura fold-and-thrust belt: a kinematic
433 model based on map-balancing. *Mémoires du Muséum national d'histoire naturelle*, 170, 235-
434 261, 1996.

- 435 Pfiffner, O. A.: *Geology of the Alps*. Chichester: John Wiley & Son, 2014.
- 436 Rime, V., Sommaruga, A., Schori, M., and Mosar, J. : *Tectonics of the Neuchâtel Jura Mountains:*
437 *insights from mapping and forward modelling*. *Swiss Journal of Geosciences*, 112, 563-578,
438 2019.
- 439 Roberts, N. M., Drost, K., Horstwood, M. S., Condon, D. J., Chew, D., Drake, H., and Haslam, R.:
440 *Laser ablation inductively coupled plasma mass spectrometry (LA-ICP-MS) U-Pb carbonate*
441 *geochronology: strategies, progress, and limitations*. *Geochronology*, 2(1), 33-61, 2020.
- 442 Roberts, N. M., Žák, J., Vacek, F., and Sláma, J.: *No more blind dates with calcite: Fluid-flow vs.*
443 *fault-slip along the Očkov thrust, Prague Basin*. *Geoscience Frontiers*, 12(4), 101143, 2021.
- 444 Sissingh, W.: *Comparative Tertiary stratigraphy of the Rhine Graben, Bresse Graben and Molasse*
445 *Basin: correlation of Alpine foreland events*. *Tectonophysics*, 300, 249–28, 1998.
- 446 Smeraglia, L., Aldega, L., Billi, A., Carminati, E., Di Fiore, F., Gerdes, A., and Vignaroli, G.:
447 *Development of an Intrawedge Tectonic Mélange by Out-of-Sequence Thrusting, Buttressing,*
448 *and Intraformational Rheological Contrast, Mt. Massico Ridge, Apennines, Italy*. *Tectonics*,
449 38(4), 1223-1249, 2019.
- 450 Smeraglia, L., Fabbri, O., Choulet, F., Buatier, M., Boulvais, P., Bernasconi, S.M., and Castorina,
451 F.: *Syntectonic fluid flow and deformation mechanisms within the frontal thrust of foreland*
452 *fold-and-thrust belt: Example from the Internal Jura, Eastern France*. *Tectonophysics*, 778,
453 <https://doi.org/10.1016/j.tecto.2019.228178>, 2020.
- 454 Sommaruga, A.: *Geology of the Central Jura and the Molasse basin: New insight into an evaporite-*
455 *based foreland fold and thrust belt*. *Mémoires de la Société Neuchâteloise de Sciences*
456 *Naturelles*, 12, pp. 176, 1997.
- 457 Sommaruga, A., Mosar, J., Schori, M., and Gruber, M.: *The role of the Triassic evaporites*
458 *underneath the North Alpine foreland*. In Soto, J., Flinch, J., and Tari, G., (Ed.), *Permo-*
459 *Triassic salt provinces of Europe, North Africa and the Atlantic Margins: tectonics and*
460 *hydrocarbon potential*, chapter 22 (IV). Elsevier, 2017.

461 Thouvenot, F., Fréchet, J., Tapponnier, P., Thomas, J. C., Le Brun, B., Ménard, G., and Paul, A.:
462 The ML 5.3 Epagny (French Alps) earthquake of 1996 July 15: a long-awaited event on the
463 Vuache Fault. *Geophysical Journal International*, 135(3), 876-892, 1998.

464 Timar-Geng, Z., Fu¨genschuh, B., Wetzel, A., and Dresmann, H.: The low temperature thermal
465 history of northern Switzerland as revealed by fission track analysis and inverse thermal
466 modelling. *Eclogae Geologicae Helvetiae*, 99, 255–270, 2006.

467 Twiss, R. J., and Moores, E. M.: *Structural geology*. Macmillan, 1992.

468 Urai, J. L., Williams, P. F., and Van Roermund, H. L. M.: Kinematics of crystal growth in
469 syntectonic fibrous veins. *Journal of Structural Geology*, 13(7), 823-836, 1991.

470 Ustaszewski, K., and Schmid, S. M.: Control of preexisting faults on geometry and kinematics in
471 the northernmost part of the Jura fold-and-thrust belt. *Tectonics*, 25, 1-26, 2006.

472 Van der Pluijm, B. A., Hall, C. M., Vrolijk, P. J., Pevear, D. R., and Covey, M. C.: The dating of
473 shallow faults in the Earth's crust. *Nature*, 412(6843), 172-175, 2001.

474 Vergés, J., Muñoz, J. A., and Martínez, A.: South Pyrenean fold and thrust belt: The role of foreland
475 evaporitic levels in thrust geometry. In *Thrust tectonics*, 255-264. Springer, Dordrecht, 1992.

476 Von Hagke, C., Cederbom, C. E., Oncken, O., Stöckli, D. F., Rahn, M. K., and Schlunegger, F.:
477 Linking the northern Alps with their foreland: The latest exhumation history resolved by low-
478 temperature thermochronology. *Tectonics*, 31(5), 2012.

479 Von Hagke, C., Oncken, O., Ortner, H., Cederbom, C. E., and Aichholzer, S.: Late Miocene to
480 present deformation and erosion of the Central Alps—Evidence for steady state mountain
481 building from thermokinematic data. *Tectonophysics*, 632, 250-260, 2014.

482 Vrolijk, P., Pevear, D., Covey, M., and LaRiviere, A.: Fault gouge dating: history and evolution.
483 *Clay Minerals*, 53(3), 305-324, 2018.

484 Woodcock, N. H., Miller, A. V. M., & Woodhouse, C. D.: Chaotic breccia zones on the Pembroke
485 Peninsula, south Wales: Evidence for collapse into voids along dilational faults. *Journal of*
486 *Structural Geology*, 69, 91-107, 2014.

